Creep-Damage Modelling for Micro Gas Turbine Combustion Chambers Lifetime Prediction

Daniele Cirigliano
German Aerospace Center (DLR)
daniele.cirigliano@dlr.de
Stuttgart, Germany

Herol Lawerence D'Souza
Ruhr University-Bochum
herollawrence@gmail.com
Bochum, Germany

Felix Grimm
German Aerospace Center (DLR)
felix.grimm@dlr.de
Stuttgart, Germany

Peter Kutne
German Aerospace Center (DLR)
peter.kutne@dlr.de
Stuttgart, Germany

Manfred Aigner
German Aerospace Center (DLR)
manfred.aigner@dlr.de
Stuttgart, Germany

ABSTRACT

Micro Gas Turbines (MGTs) are nowadays largely used for electrical and thermal energy production in small buildings and households. Their reliability and compactness allow them to operate for thousands of hours with minimal maintenance. However, the long exposure at high temperatures in combustion chambers can promote creep, which can induce thermal fatigue and potential failure of these components. Creep-induced damage in MGTs has not yet been thoroughly investigated, due to the lack of numerical tools able to model these strongly coupled phenomena. This study presents the development of a Fortran-based subroutine integrated into ANSYS APDL. The code allows for a life assessment based on the Lemaitre-Chaboche creep damage model. Secondary creep and stress relaxation are modeled for the high-temperature resistant alloy Inconel718. A new set of temperature-dependent parameters for the Norton equation is provided, and the method to obtain these parameters from creep rupture tests is outlined. The model is validated and shows good agreement with experimental data. The subroutine correctly reproduces visco-plasticity, stress relaxation and damage under typical MGTs operating temperatures. This model constitutes the foundation of a life-assessment analysis for combustion chambers. The results highlight the impact of temperature and creep on the component's life and the importance of integrating life assessment analysis into the preliminary design of combustion chambers.

INTRODUCTION

Micro Gas Turbines (MGTs) for co-, tri- or polygeneration are becoming progressively more widespread because of their reliability, flexibility, compactness and very low NOx emissions (Sun et al., 2012). Despite the on-going energy transition and the short-term impact due to the lingering COVID-19 pandemic, the global production of MGTs (especially in Europe) shows a promising increasing trend for the next decade (Palmer, 2021). Although the electrical efficiency is generally lower than the one for similar size internal combustion engines (Ofualagba, 2012), the high total efficiency of MGTs, which can reach 80% thanks to the extraction of the high exhaust gases thermal content through a recuperator (Beith, 2011) is one of the main reason for their increasing adoption. Moreover, exhaust heat can be further extracted by means of a heat exchanger for the production of hot water.

However, if on one side recuperation is beneficial for the overall system efficiency, on the other side it reduces the ability to cool down the hot mechanical components, such as the combustion chamber, being the inlet air largely warmer than what it would be without recuperation. In MGTs, the air entering the combustion chamber is often above 650°C (Enagi et al., 2017). The lower cooling capability, in addition to the higher flame temperature due to warmer inlet gases, causes very high temperatures in the metal components of the combustion chamber, with peaks of 1200 K in some cases (Cirigliano et al., 2020). Frequent starts and stops induce mechanical stresses at the boundary between materials due to their different thermal expansion, which, if taking place too fast, may cause local permanent plastic deformations. Moreover, long exposure at high temperatures in combustion chambers can promote creep, which can induce thermal fatigue and potential failure of these components. The accumulation of damage in combustion chambers can hence be divided into two categories: the plasticity taking place during transient states (maneuvers, starts and stops) and the viscoplastic-based damage (creep damage) at steady state operation.

It is then necessary to take into account the material degradation due to the progressively increasing viscoplastic deformation; this can be done by adding a scalar parameter to the mechanical model. Commercial Finite Element Methods (FEM) codes, like ANSYS, allow the user to write their custom mechanical model. In this work, the development of a Fortran-based subroutine integrated into ANSYS APDL is presented. On so doing, creep, damage, and material degradation can be modeled. In this work, Lemaitre-Chaboche creep damage model is adopted (Lemaitre and Chaboche, 1978). Secondary creep and isotropic hardening are modeled for the high-temperature resistant alloy Inconel 718. The material degradation is considered by coupling the Young's modulus with the introduced damage.

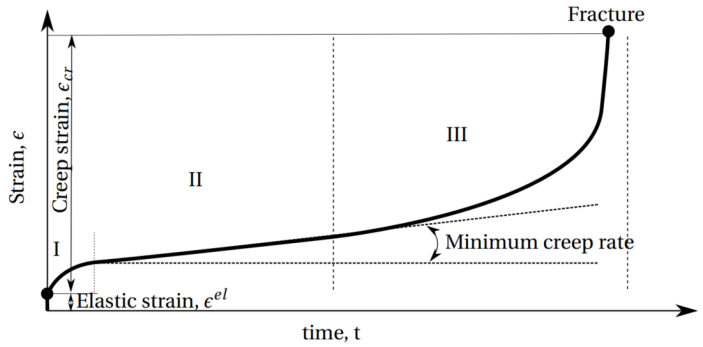

Figure 1 Typical creep strain vs. time curve showing the three stages of creep.

The novelty of this paper consists in the determination of Norton coefficients for Inconel 718, which instead of being assumed constant, are temperature dependent and based on experimental data. It is shown that the creep model and subroutine based on these new coefficients correctly reproduces creep, stress relaxation and damage under typical MGT operating temperatures. This model constitutes the foundation of a life-assessment analysis for combustion chambers under creep damage.

NUMERICAL METHODS

Creep Modelling

Creep is described as a time-dependent deformation of a material subjected to high temperature and loads below its yield strength for an extended period of time. Temperature, stress, time and material properties influence the rate of creep deformation. The creep phenomena is mainly divided into three stages; i.e. primary I, secondary II, and tertiary III. The three stages correspond to strain rates that are decreasing, constant, and increasing, respectively. Figure. 1 depicts a typical creep strain versus time curve. The stage I in the curve indicates the primary creep where the creep strain rate decreases to a minimum value, due the fact that the material is experiencing an increase in creep resistance, attributed to a reduction in the density of free dislocations. The stage II is known as steady-state creep or secondary creep. This regime is also termed as a state of balance between the rate of dislocation generation and rate of recovery, where the former contributes to hardening and the latter to softening of the test material (Abe, 2014). In the tertiary creep stage, the creep rate increases rapidly until failure. This stage describes a softening stage, where the cracks are formed and propagate along the grain boundaries (Betten, 2008). In addition, the microscopic voids accumulate within the material, resulting in a decrease in the effective cross-sectional area (i.e. Necking), which raises the effective stress.

In order to capture the damage caused by creep, the modified Lemaitre-Chaboche model (Chaboche and Rousselier, 1983), (Lemaitre, 1985) is used in this study. The effective stress concept Lemaitre and Chaboche (1978) defines the creep damage D_{cr} starting from the effective section $\tilde{S}$ and the effective uniaxial stress σ:

$$\tilde{\sigma} = \frac{S}{\tilde{S}}\sigma = \frac{\sigma}{1 - D_{cr}} \tag{1}$$

where D_{cr} represents the macroscopic effect of the mechanical degradation due to creep voids, and $\tilde{S} = S - S_{voids}$. Hence, strictly speaking, D_{cr} would be defined as $D_{cr} = S_{voids}/S$. Given the difficulty to obtain a reliable measure of S_{voids} during operation, it is more practical to describe the status of D_{cr} as the integral of its time evolution:

$$D_{cr}(t) = \int_0^t \dot{D}_{cr}(t)dt. \tag{2}$$

Equivalent Von-Mises stress and equivalent strain are defined in terms of their stress and strain components:

$$\sigma_{eq} = \sqrt{\frac{(\sigma_1 - \sigma_2)^2 + (\sigma_2 - \sigma_3)^2 + (\sigma_3 - \sigma_1)^2}{2}} \tag{3}$$

$$\varepsilon_{eq} = \frac{\sqrt{2}}{3}\sqrt{(\varepsilon_1 - \varepsilon_2)^2 + (\varepsilon_2 - \varepsilon_3)^2 + (\varepsilon_3 - \varepsilon_1)^2}. \tag{4}$$

The total equivalent strain ε_{eq} is given by the sum of elastic, plastic, thermal and creep equivalent strains:

$$\varepsilon_{eq} = \varepsilon_{eq}^{el} + \varepsilon_{eq}^{pl} + \varepsilon_{eq}^{th} + \varepsilon_{eq}^{cr}. \tag{5}$$

Creep mechanisms can generally be grouped into two categories: diffusion creep and dislocation creep. Diffusion creep is dominant at lower stresses, and is caused by the movement of vacancies; dislocation creep is present at higher stresses and is caused by the movement of dislocations through the lattice. When a dislocation encounters an obstacle (for example another defect), the

C_1	C_2	C_4
$2.147 \cdot 10^{-7}$	10.171	50825.89

Table 1 Norton coefficients for Inconel 718 according to (Liu et al., 2015).

a_0	a_1	a_2	r	z	A
13.2478	$0.7865 \cdot 10^{-4}$	$0.1924 \cdot 10^{-3}$	13.19	733.25	1209

Table 2 Material constants for damage evolution equation.

former can either climb it (at mid stresses) or glide through it (at high stresses). The creep mechanisms acting in a material can be identified for a range of stresses and temperatures in a deformation map, according to the methods described by Frost and Ashby (1982). A deformation map of Inconel 718 is not available to the authors, but similar Nickel-based superalloys, such as IN738LC Carey et al. (1990) or MAR-M-200 Cieśla et al. (2016), show the onset of dislocation creep at half of the melting point (about 600 $°C$) and at stresses above 50 MPa. The operative conditions at which MGT combustion chambers are operated (metal temperature and stresses due to thermal strains) lay above these values. Moreover, it has been shown in other studies that the validity of creep power laws, for example the Norton law, can be extended by accounting for temperature-dependent parameters Golan et al. (1996), Alain (1998) or by introducing recovery processes associated to the dislocation structure Das et al. (2022). Barbosa et al. (1988) used physics-based four stress- and temperature-dependent parameters to describe creep curves. McLean et al. (1992) modelled creep curves of single crystal superalloys using eight temperature- and stress-dependent parameters. On so doing, power law can be used to describe the creep behavior over an extensive range of stress and temperature. For these reasons, this work aims to model dislocation creep only, and to adapt the Norton law material parameters to different temperatures.

The derivative of creep equivalent strain in time (primary and tertiary creep) can be described in the form of its dependency on equivalent stress, temperature and either creep strain or time, by means of a power law:

$$\dot{\varepsilon}_{eq}^{cr} = C_1 \sigma_{eq}^{C_2} \varepsilon_{eq}^{cr\,C_3} e^{-C_4/T}, \quad or \quad \dot{\varepsilon}_{eq}^{cr} = C_1 \sigma_{eq}^{C_2} t^{C_3} e^{-C_4/T} \tag{6}$$

where T is the temperature and t is the time. For secondary creep, however, the strain rate is constant, hence, $C_3 = 0$:

$$\dot{\varepsilon}_{eq}^{cr} = C_1 \sigma_{eq}^{C_2} e(-C_4/T), \tag{7}$$

where C_1, C_2 and C_4 are material constants whose values are determined using creep tests. Equation 7 is the most important and widely used formulation to predict the secondary creep and is known as Norton power law. Table 1 shows the values of C_1, C_2 and C_4 for Inconel 718 according to (Liu et al., 2015) and based on creep test data (Li et al., 2010). Note that for these parameters, stress is expressed in MPa, temperature in K, and strain in units per hour.

The creep damage evolution is given by:

$$\dot{D}_{cr} = \left(\frac{\sigma_{eq}}{A}\right)^r (1 - D_{cr})^{-k}, \tag{8}$$

where D_{cr} is the scalar creep damage parameter. $\dot{D}_{cr}$ is expressed in units per second and k is given by:

$$k = a_0 + a_1(\sigma_{eq} - z) + a_2(\sigma_{eq} - z)^2, \tag{9}$$

where a_0, a_1, a_2, z, r and A are material constants which are determined again by creep tests. For Inconel 718 these values are reported in Tab. 2 (Zhang, 1995).

The scalar creep damage variable D_{cr} is zero for undamaged material and increases in time with Eq. 8 up to an arbitrary value, usually 1, at which the material is assumed to fail. Basing on the damage theory of (Kachanov, 1999) and taking into account the concept of effective stress (Rabotnov et al., 1970) and the principle of strain equivalence (Lemaitre and Chaboche, 1978), changes in mechanical behavior can be measured through the evolution of the elastic modulus Lemaitre (1985):

$$E = E_0(1 - D_{cr}), \tag{10}$$

where E is the effective elastic modulus and E_0 is the Young's modulus of undamaged material. By differentiating Eq. 10 in time, one obtains:

t_r (h)	T (°C)	B	α
< 11000	≥ 593	2.142	1.151
< 11000	≤ 593	34.182	1.443
≥ 11000	any	2.142	1.151

Table 3 B and α parameters.

T (°C)	C_1	C_2	C_4
427	$1.10 \cdot 10^{-9}$	21.8	109 000
482	$3.00 \cdot 10^{-9}$	15.8	84 000
538	$4.00 \cdot 10^{-9}$	14.4	81 000
593	$2.00 \cdot 10^{-9}$	12.3	71 000
649	$1.00 \cdot 10^{-7}$	5.4	34 500
704	$5.00 \cdot 10^{-6}$	3.7	29 000
760	$2.00 \cdot 10^{-7}$	4.5	28 000

Table 4 Norton equation coefficients at different temperatures for Inconel 718.

$$\dot{E} = -E_0 \dot{D}_{cr} = -E_0 \left(\frac{\sigma_{eq}}{A} \right)^r (1 - D_{cr})^{-k}. \tag{11}$$

By remembering the constitutive relation between σ, ε_{el} and the elasticity matrix $[D]$, which contains E (Chandrupatla and Belegundu, 2012), one can derive:

$$\dot{\sigma} = [\dot{D}]\varepsilon^{el} + [D]\dot{\varepsilon}^{el}. \tag{12}$$

Equation 12, together with Eq. 7 and 8, constitute a system of nonlinear differential equations in σ_{eq}, D_{cr} and ε^{cr}_{eq}, where T can be constant or vary with time too. Also by remembering the fact that ε^{el}_{eq} and ε^{cr}_{eq} are related by Eq. 5, it is clear how this highly coupled problem needs to be solved by a dedicated code.

Material Parameters Identification

In applying the Norton formulation (Eq. 7) to the analysis of structures one should bear in mind that the material parameters C_1, C_2 and C_4 are obtained by interpolating experimental creep tests, hence their validity is limited to the narrow range of stresses and temperatures the tests were conducted. In the previous section, a set of these parameters is proposed in Tab. 1. However, the use of only three constants to cover the whole spectrum of stresses and temperatures a structure can be subjected to might introduce relevant inaccuracies in the model. For this reason, in this paper a whole new set of parameters was derived from the creep tests of Inconel 718 at different temperatures performed by (Brinkman et al., 1991). In Fig. 2, the results of the creep tests are shown. In this section, a method to derive Norton parameters from creep tests is highlighted.

Since the secondary creep stage is characterized by a constant creep strain rate, one can assume $d\varepsilon^{cr}_{eq}/dt \simeq \varepsilon^{cr}_{eq,ss}/t_{ss}$, where $\varepsilon^{cr}_{eq,ss}$ and t_{ss} are the equivalent creep strain and the time to the onset of tertiary creep, respectively. Hence, the Norton relation (Eq. 7) can be rewritten in the form:

$$\sigma_{eq} = \left(\frac{\varepsilon^{cr}_{eq,ss} \, exp(C_4/T)}{C_1 \, t_{ss}} \right)^{\frac{1}{C_2}} \tag{13}$$

where T, t_{ss} and σ_{eq} are expressed in Kelvin, hours and MPa respectively. The time to the onset of tertiary creep can be related to the time to rupture for Inconel 718 by (Brinkman et al., 1991):

$$t_{ss} = A t_r^{\beta}. \tag{14}$$

with A=0,442 and β=1,04 up to t_r=10^5 hours, and A=0,7 and β=1 above. Relating $\varepsilon^{cr}_{eq,ss}$ with the creep strain to rupture, $\varepsilon^{cr}_{eq,r}$, remains an harder task, due to the large amount of scatter which is typical in creep measurements. For temperatures between 650°C and 760°C, some creep tests indicate $\varepsilon^{cr}_{eq,r}$ between 3% and 9%, increasing with temperature (Caliari et al., 2016; Kim et al., 2008; Sugahara et al., 2012). A more handy correlation is given again by (Brinkman et al., 1991):

$$\varepsilon^{cr}_{eq,ss} = 0.2 + A \, B t_r^{(\beta - \alpha)}, \tag{15}$$

where A and β are the same as shown above, 0.2 is the elastic strain offset, and B and α are reported in Tab. 3.

In this way, the determination of temperature-dependent parameters C_1, C_2 and C_4 can finally take place as follows:

1. Obtain from creep tests points (σ, t_r) at different temperatures;
2. compute t_{ss} from Eq. 14 with the corresponding A, β;
3. compute $\varepsilon^{cr}_{eq,ss}$ from Eq. 15 with the corresponding B, α;

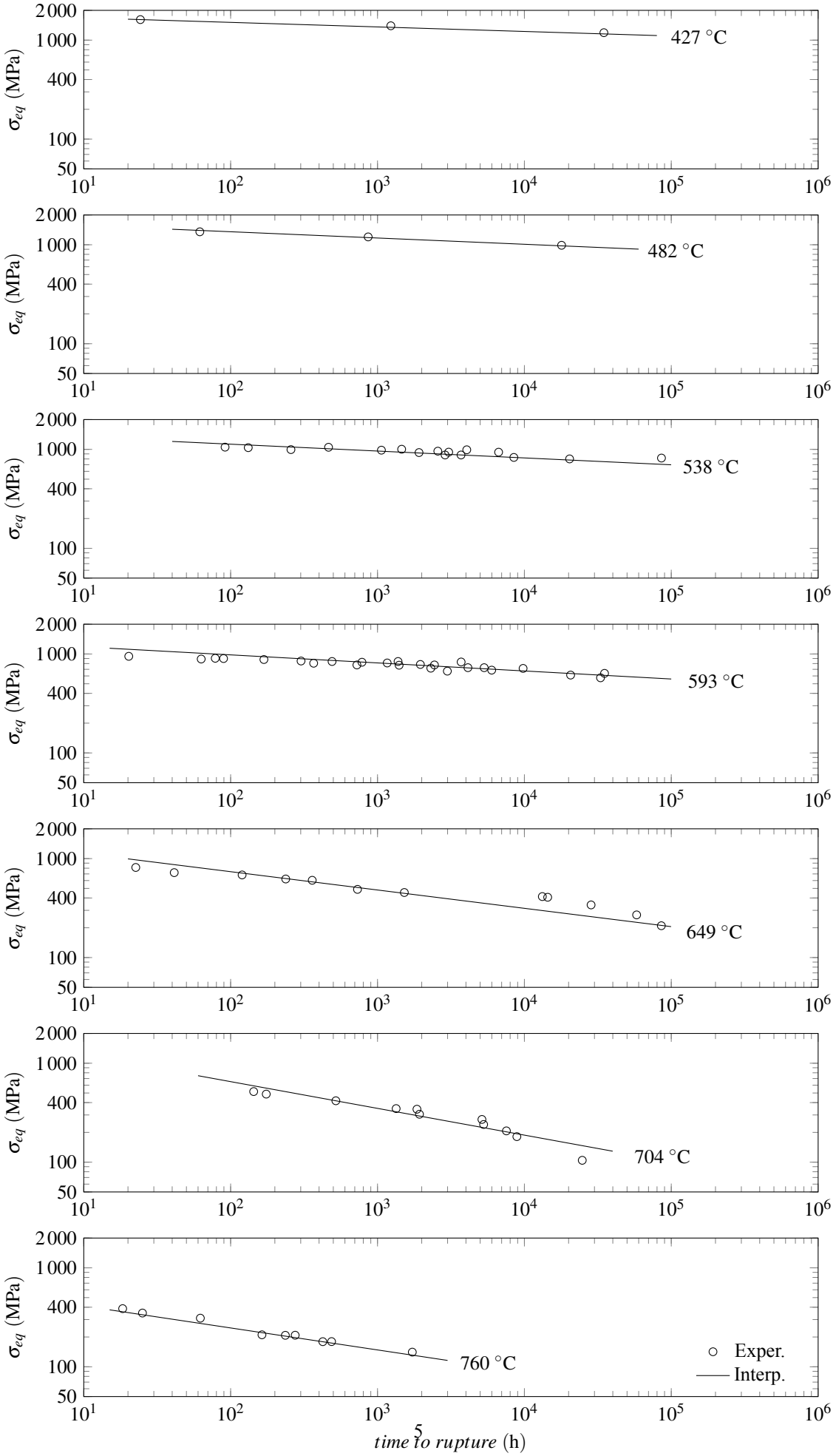

Figure 2 Creep-rupture lifetime data and numerical interpolation for Inconel 718.

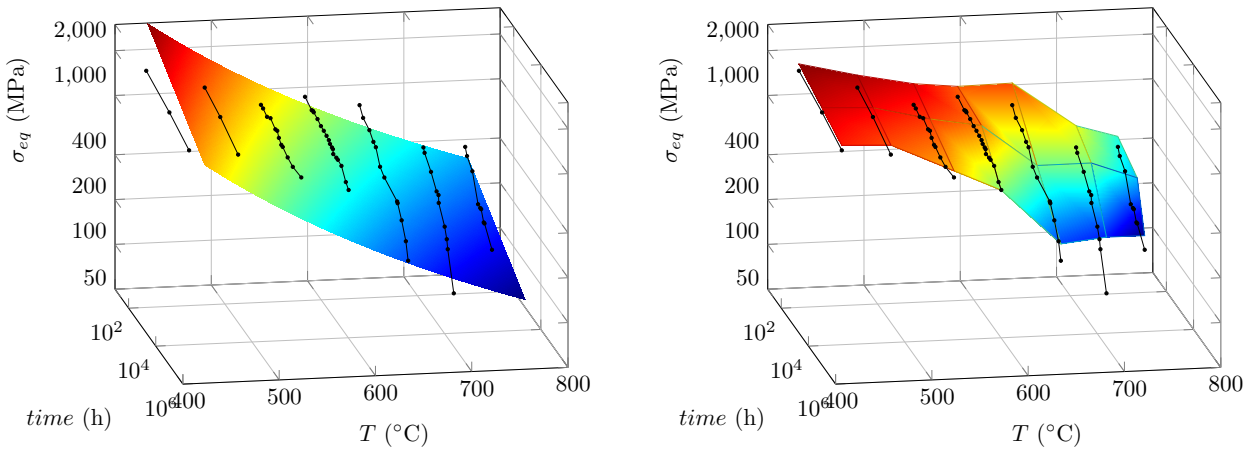

(a) *Constant coefficients (Tab. 1).*

(b) *Variable coefficients (Tab. 4).*

Figure 3 Creep-tests can be plotted in a three-dimensional space, where each point is represents a test conducted at a specific σ_{eq}, t_r and T. By computing the creep strain with the Norton law, a 3D surface can be obtained and overlapped to experimental data. A comparison between constant parameters (a) and temperature-dependent parameters (b) shows a much better fit of the latter.

4. substitute t_{ss} and $\varepsilon^{cr}_{eq,ss}$ in Eq. 13;
5. for every temperature T, find the values $\{C_1, C_2, C_4\}$ giving a σ_{eq} as close as possible to the one of the tests (point 1).

The key point of this approach is noting that creep tests are performed at constant stress, hence, one can use the same σ_{eq} of the creep rupture tests to relate the t_r to the state on onset of tertiary creep, t_{ss} and $\varepsilon^{eq}_{eq,ss}$ of Norton formulation, which is generally not known. The new set of parameters for Inconel 718 is presented in Tab. 4. By applying these parameters in Eq. 13, interpolating curves are generated and plotted in Fig. 2, showing excellent fit. A comparison between the use of constant parameters and temperature-dependent parameters can be well appreciated in a 3D space (Fig. 3).

User Programmable Feature USERMAT in ANSYS

In this section, the implementation of a damage-based material model in the commercial software ANSYS APDL is outlined. User Programmable Features (UPFs) are a highly effective and flexible tool to tailor the behavior of the APDL program to suit individual requirements. This is performed by writing a custom subroutine in the C, C++, or Fortran programming languages. One of such subroutines is USERMAT, which is particularly used to define non-linear stress-strain relationships of elastic-plastic materials, custom damage evolution and creep laws, like in this study.

USERMAT subroutine is called at every iteration and executed on each element of the computational grid. The input parameters, such as loads and temperature, are defined by the user during the modelling step. Current stresses, strains and strain increments are the inputs at the start of the timestep. At each iteration, a new elastic, plastic, thermal and creep strain, an effective Young's modulus and damage evolution are computed based on the constitutive equations and material model described in the previous sections. USERMAT then updates the stresses and the material Jacobian matrix and these values are sent back to the main Finite Element code as outputs (Lin, 1999). The status of every element is checked at every time increment using a strength lifetime failure criterion: when the maximum damage of the structure reaches a threshold value, the subroutine is stopped and the present time is recorded as the lifetime of the component. In this analysis, $D_{cr} = 0.4$ is considered as the the maximum allowable damage.

The geometry chosen is a rectangular bar of Inconel 718 alloy with a base of 10x10 mm and a length of 100 mm. The bar is discretized with 2 hexahedral elements for each short side and with 20 along the length (80 elements in total). Since the application of the present work is three-dimensional and plain strain, SOLID186 elements (20 nodes each, second-order shape functions) are used. The bar is fixed at one end and a displacement is applied to the opposite end to obtain the uni-axial stress state. Material properties of Inconel 718 such as density, thermal expansion coefficients and Young's modulus (of undamaged material) are taken from data sheets (VDM Metals, 2020).

RESULTS AND DISCUSSION

The application of the described UPF using the temperature-dependent coefficients is presented in this section. Temperature is set to 750 K. The comparison between the experimental tests, the Norton-Damage model with constant parameters of (Liu et al., 2015) and the Norton-Damage model of this analysis is depicted in Fig. 4.

In the experiments, a displacement is applied to one end in order to generate an initial stress of 700 MPa; shortly after, the stress relaxes to a much lower value, around 635 MPa, showing the typical primary creep phase. Afterwards, the stress stabilizes

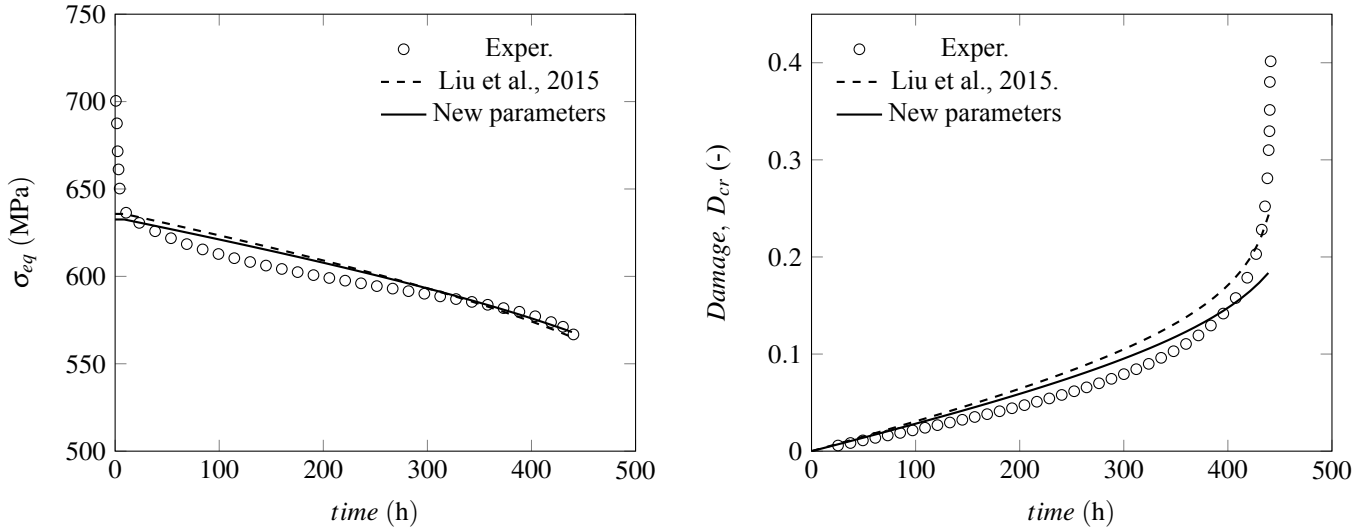

Figure 4 Comparison between experimental data, the use of the constant parameters from (Liu et al., 2015) and the new, temperature-dependent parameters, at 750K and initial σ=700 Mpa.

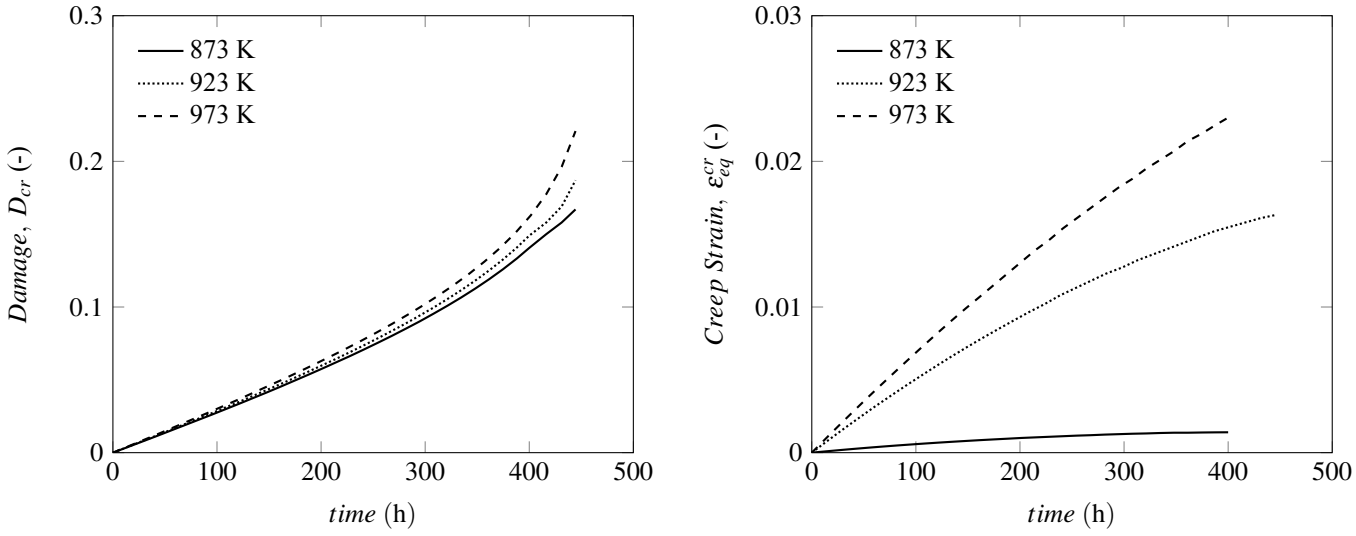

Figure 5 Damage and creep strain at three different temperatures and initial σ=650 Mpa.

and slowly decreases, due to further stress relaxation. Finally, a rapid decrease in the cross-sectional area of the probe brings the material to failure.

For the two simulations, since the Norton equation only models the secondary creep, an initial $\sigma = 635$ MPa is set. The decrease of equivalent stress is due to a decrease in effective Young's modulus, in turn due to damage accumulation, as expected (see Eq. 10). Both the stress decrease and the damage increase are represented with good accuracy when compared to the experimental data, except from the areas at the very beginning and at the end of the simulations, where the stress decreases relatively fast. Those are the areas corresponding to primary and tertiary creep. It must be remembered that this UPF is developed to model secondary creep, hence, the high strain rates typical of primary and tertiary creep are out of the scope of this paper.

The temperature-dependent parameters allow the user to span over a wider range of (in particular to higher) temperatures, compared to those parameters of (Liu et al., 2015), which are optimized for 750 K only. As an example, creep strain and damage over time at three different temperatures and for an initial stress of 650 MPa are shown in Fig. 5. It can be seen that temperature has an enormous impact on creep and on creep strain, as expected. Higher temperatures promote a much faster creep deformation. This is depicted well from the picture on the right. On the left, the damage shows again a non-linear increasing trend with time. Since the Chaboche-Lemaitre damage D_{cr} depends on equivalent stress only (at least directly, see Eqs. 8 and 9), the damage evolution is, in the first phase, very similar for all the temperatures. Over time, the damage increases more at higher temperatures, both due to higher creep and lower Young's modulus with temperature.

CONCLUSIONS

In this paper, a method for the determination of temperature-dependent Norton coefficients for Inconel 718 was shown. The procedure takes rupture creep test data as input. The so obtained coefficients are then implemented in a User Programmable Feature inside the ANSYS APDL environment, enabling the user to write a custom mechanical model. In this study, secondary creep together with material damage and Young's modulus reduction were combined.

The results show excellent agreement with the experimental data, strictly concerning the secondary creep portion of the tests. The UPF allows the simulation of creep damage in a wide range of temperatures, in particular up to $760°C$, which are close to the temperatures typical of a gas turbine combustion chamber. This method has the potential to be extended to even higher temperatures, if creep tests are provided. The range $760\text{-}1000°C$ is currently under development.

This study constitutes the foundation to explore the life of Inconel 718 structures exposed at high temperature creep, where stress relaxation, damage and creep are taken into account for a realistic representation of this coupled problem. The direct application of this USERMAT subroutine in ANSYS to MGT combustion chambers is currently under development and will be published on basis of a separate study.

NOMENCLATURE

Latin Symbols		**Greek Symbols**	
$[D]$	elasticity matrix	ε	strain tensor
D_{cr}	creep damage	ε_{eq}	equivalent total strain
E	effective Young's modulus	ε_{eq}^{cr}	equivalent creep strain
E_0	undamaged Young's modulus	$\varepsilon_{eq,ss}^{cr}$	eq. creep strain at III creep onset
MGT	Micro Gas Turbine	ε_{eq}^{el}	equivalent elastic strain
t_r	rupture time	ε_{eq}^{pl}	equivalent plastic strain
t_{ss}	time at III creep onset	ε_{eq}^{th}	equivalent thermal strain
UPF	User Programmable Feature	σ	stress tensor
		σ_{eq}	equivalent stress

REFERENCES

Abe, F. (2014), Development of creep-resistant steels and alloys for use in power plants, *in* A. Shirzadi and S. Jackson, eds, 'Structural Alloys for Power Plants', Woodhead Publishing Series in Energy, Woodhead Publishing, pp. 250–293.
URL: *https://doi.org/10.1533/9780857097552.2.250*

Alain, I. (1998), 'The correlation between the power-law coefficients in creep: The temperature dependence', *Journal of Materials Science - J MATER SCI* **33**, 3201–3206.

Barbosa, A. L., Taylor, N. G., Ashby, M. F., Dyson, B. F. and Mclean, M. (1988), 'A model based computer analysis of creep data (cripsen): Applications to nickel-base superalloys', *Superalloys* pp. 683–692.

Beith, R. (2011), 'Small and micro combined heat and power (chp) systems', *Woodhead Publishing Series in Energy* .

Betten, J. (2008), *Creep Mechanics*, Springer Science & Business Media.

Brinkman, C., Booker, M. and Ding, J. (1991), 'Creep and creep-rupture behavior of alloy718'.

Caliari, F. R., Candioto, K. C. G., Couto, A. A., Nunes, C. Â. and Reis, D. A. P. (2016), 'Effect of double aging heat treatment on the short-term creep behavior of the inconel 718', *Journal of Materials Engineering and Performance* **25**(6), 2307–2317.

Carey, J., Sargent, P. and Jones, D. (1990), 'Deformation mechanism map for in738lc superalloy', *Journal of Materials Science Letters* **9**, 572–575.

Chaboche, J. L. and Rousselier, G. (1983), 'On the plastic and viscoplastic constitutive equations—part i: Rules developed with internal variable concept', *Journal of Pressure Vessel Technology* **105**(2), 153–158.
URL: *https://doi.org/10.1115/1.3264257*

Chandrupatla, T. R. and Belegundu, A. D. (2012), *Introduction to Finite Elements in Engineering*, 4 edn, Pearson.

Cieśla, M., Mańka, M., Binczyk, F. and Gradoń, P. (2016), 'Creep behaviour of modified mar-247 superalloy', *Archives of Metallurgy and Materials* **61**.

Cirigliano, D. et al. (2020), 'Thermo-structural analysis of a micro gas turbine jet- and recirculation- stabilized combustion chamber.', *Proceedings of ASME Turbo Expo 2020* **10B**(GT2020-16285).

Das, Y., Fernandez-Caballero, A., Elmukashfi, E., Jazaeri, H., Forsey, A., Hutchings, M. T., Schweins, R. and Bouchard, P. J. (2022), 'Stress driven creep deformation and cavitation damage in pure copper', *Materials Science and Engineering: A* **833**, 142543.
URL: *https://www.sciencedirect.com/science/article/pii/S0921509321018037*

Enagi, I. I., Al-attab, K. and Z.A.Zainal (2017), 'Combustion chamber design and performance for micro gas turbine application.', *Fuel Processing Technology* **166**(2), 258–268.

Frost, H. and Ashby, M. (1982), *Deformation-Mechanism Maps*, Pergamon Press.

Golan, O., Arbel, A., Eliezer, D. and Moreno, D. (1996), 'The applicability of norton's creep power law and its modified version to a single-crystal superalloy type cmsx-2', *Materials Science and Engineering: A* **216**(1), 125–130.
URL: *https://www.sciencedirect.com/science/article/pii/0921509396104007*

Kachanov, L. M. (1999), 'Rupture time under creep conditions', *International journal of fracture* **97**(1–4), 11–18.

Kim, D.-H., Kim, J.-H., Sa, J.-W., Lee, Y.-S., Park, C.-K. and Moon, S.-I. (2008), 'Stress rupture characteristics of inconel 718 alloy for ramjet combustor', *Materials Science and Engineering: A* **483-484**, 262–265. 14th International Conference on the Strength of Materials.
URL: *https://doi.org/10.1016/j .msea.2006.12.159*

Lemaitre, J. (1985), 'A continuous damage mechanics model for ductile fracture', *Journal of Engineering Materials and Technology* **107**(1), 83–89.
URL: *https://doi.org/10.1115/1.3225775*

Lemaitre, J. and Chaboche, J.-L. (1978), 'Aspect phénoménologique de la rupture par endommagement', *Journal de Mecanique Appliquee* **2**(3), 317–365.

Li, L., Song, Y. and Huang, X. (2010), 'Analysis on creep and creep life of rotors connecting bolts', *Technology & New Process* **6**, 75–79.

Lin, G. (1999), 'Ansys user material subroutine usermat', *ANSYS, Canonsburg, PA* .

Liu, D., Li, H. and Liu, Y. (2015), 'Numerical simulation of creep damage and life prediction of superalloy turbine blade', *Mathematical Problems in Engineering* **2015**. Article ID 732502, 10 pages.
URL: *https://doi.org/10.1155/2015/732502*

McLean, M., Ghosh, R., Curtis, R., Basu-Conlin, U. and Winstone, M. (1992), 'Anisotropy of high temperature deformation of single crystal superalloys - constitutive law, modelling and validation', *The Minerals, Metals and Materials Society* **Superalloys 1992**, 609–618.

Ofualagba, G. (2012), 'The modeling and simulation of a microturbine generation system.', *International Journal of Scientific & Engineering Research* **2**(2), 1–7.

Palmer, C. (2021), 'Eworldwide gas turbine market report 2022', *Turbomachinery Magazine, Handbook 2022* .
URL: *https://www.turbomachinerymag.com/view/worldwide-gas-turbine-market-report-2022*

Rabotnov, Y. N., Leckie, F. A. and Prager, W. (1970), 'Creep problems in structural members', *Journal of Applied Mechanics* **37**(1), 249–249.
URL: *https://doi.org/10.1115/1.3408479*

Sugahara, T., Martinolli, K., Reis, D. A., de Moura Neto, C., Couto, A. A., Neto, F. P. and Barboza, M. (2012), Creep behavior of the inconel 718 superalloy, *in* 'Defect and Diffusion Forum', Vol. 326, Trans Tech Publ, pp. 509–514.

Sun, L. et al. (2012), 'Numerical Simulation of a Complete Gas Turbine Engine With Wet Compression', *Journal of Engineering for Gas Turbines and Power* **135**(1). 012002.
URL: *https://doi.org/10.1115/1.4007366*

VDM Metals (2020), 'VDM Alloy 718', *Material Data Sheet No. 4127, Rev. 02* .
URL: *https://www.vdm-metals.com/fileadmin/user_upload/Downloads/Data_Sheets/Data_Sheet_VDM_Alloy_718.pdf*

Zhang, L. (1995), Research of fatigue failure on high-temperature parts based on damage mechanics, PhD thesis, Beijing University of Aeronautics and Astronautics.